ISSN 1070-3284, Russian Journal of Coordination Chemistry, 2019, Vol. 45, No. 10, pp. 680–688. © Pleiades Publishing, Ltd., 2019.
Russian Text © The Author(s), 2019, published in Koordinatsionnaya Khimiya, 2019, Vol. 45, No. 10, pp. 584–592.

Comparison of Experimental and Experimental–Theoretical Topological Characteristics of the Electron Density in the Crystalline Complex η⁶-[3-Acetyltetrahydro-6-Phenyl-2*H*-1,3-oxazine]tricarbonylchromium(0)

G. K. Fukin[a], *, E. V. Baranov[a], A. V. Cherkasov[a], R. V. Rumyantcev[a], A. N. Artemov[b], and E. V. Sazonova[b]

[a] *Razuvaev Institute of Organometallic Chemistry, Russian Academy of Sciences, Nizhny Novgorod, 603600 Russia*
[b] *Lobachevskii State University, Nizhny Novgorod, Russia*
**e-mail: gera@iomc.ras.ru*

Received March 5, 2019; revised April 1, 2019; accepted April 10, 2019

Abstract—Experimental and experimental–theoretical studies (using the molecular invariom) of the electron density distribution are performed for the η⁶-[3-acetyltetrahydro-6-phenyl-2*H*-1,3-oxazine]tricarbonylchromium(0) complex. The topological characteristics of the electron density ($\rho(\mathbf{r})$, $\nabla^2\rho(\mathbf{r})$) at the critical points (3, −1) coincide in the experimental and experimental–theoretical distributions within the "transferability indices." The experimental–theoretical study more reliably localizes the "expected" critical points (3, −1) between the chromium atom and arene ligand.

Keywords: high-resolution X-ray diffraction analysis, molecular invariom, R. Bader's theory "Atoms in Molecules," transferability of topological parameters of electron density

DOI: 10.1134/S1070328419090045

INTRODUCTION

The study of the electron density distribution according to high-resolution X-ray diffraction analysis is a very useful tool for the solution of many chemical problems [1, 2]. However, high requirements are imposed on the crystals used in high-resolution studies. These should be single crystals of a very high quality with a high reflection ability. Note that the task of obtaining a single crystal for a high-resolution experiment is often special and labor-consuming, which appreciably restricts the experimental study of the electron density in practically important compounds. The concept of invarioms (aspherical atom scattering factor) has recently been proposed [3]. In fact, this is a combined experimental–theoretical approach to study the electron density topology that requires no high-angle data. This approach excellently recommended itself to reveal a relationship between the structure and physicochemical properties for organic and inorganic salts, as well as radicals [4–7]. The next step of the development of the invariom concept was the molecular invariom (whole-molecule aspherical scattering factor) used for the correct identification of metal atoms in coordination compounds [8, 9] and for analyzing agostic interactions in the $[Cp_2FeH](PF_6)$ complex [10]. In addition, the whole-molecule invariom was used to estimate the populations of the *d* orbitals [11].

In this work, we compare the topological characteristics of the electron density at the critical points (3, −1) in the coordination sphere of the metal atom obtained from high-resolution X-ray diffraction analysis data and using the whole-molecule invariom for η⁶-[3-acetyltetrahydro-6-phenyl-2*H*-1,3-oxazine]tricarbonylchromium(0) (**Ia**).

EXPERIMENTAL

Complex **Ia** was synthesized by the direct reaction of triammine(tricarbonyl)chromium $(NH_3)_3Cr(CO)_3$ in dioxane with 3-acetyl-6-phenyl-2*H*-1,3-oxazine prepared using a known procedure [12].

High-resolution X-ray diffraction analysis of complex **Ia** was carried out at 100 K on a Bruker D8 Quest diffractometer (graphite monochromator, MoK_α radiation, $\lambda = 0.71073$ Å). Experimental sets of intensities were integrated using the SAINT program [13]. The SADABS program [14] was used to apply absorption corrections. The structure was solved by a direct method and refined by full-matrix least squares for F^2 using the SHELXTL program package [15]. All non-hydrogen atoms were refined in the anisotropic

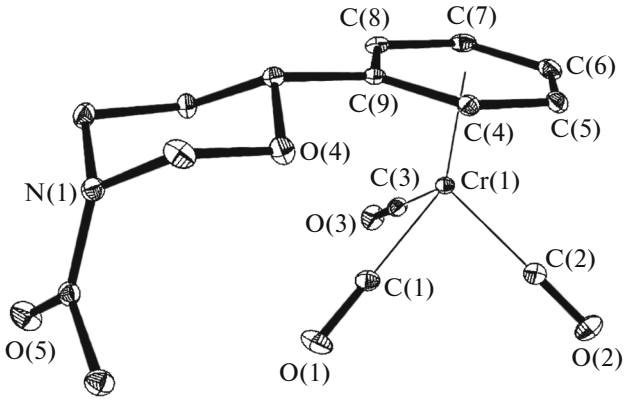

Fig. 1. Molecular structure of complex **Ia**.

approximation. Hydrogen atoms were placed in geometrically calculated positions and refined isotropically in the riding model.

The multipole refinement of complex **Ia** was carried out within the Hansen–Coppens formalism [16] using the MoPro program package [17]. Before multipole refinement, all hydrogen atoms in the high-resolution X-ray diffraction studies were normalized to the ideal distances obtained in neutron diffraction analyses [18]. The level of the multipole expansion was hexadecapole for chromium atoms, octapole for all non-hydrogen atoms, and dipole for hydrogen atoms. All bound pairs of atoms satisfied the Hirshfeld rigid-bond criteria [19]. The topological analysis of the experimental function $\rho(\mathbf{r})$ was carried out using the WINXPRO program package [20].

The low-resolution set of experimental X-ray diffraction data for complex **Ia** was used to obtain the experimental–theoretical electron density. The geometry optimization of an isolated molecule of complex **Ib** was performed by the density functional method (B3LYP/aug-cc-pVDZ [21–25]) taking into account dispersion interactions in the Grimme model [26, 27] using the Gaussian 09 program package [28]. The multiplicity of the complex was equal to 1. Then we placed the optimized molecule of complex **Ib** into a pseudocubic cell ($a = 30$ Å) (space group $P\bar{1}$), and the theoretical structural amplitudes ($\sin\theta/\lambda = 1.155$ Å^{-1}) were calculated using the Tonto program [29]. The populations of the spherically symmetrical valence shell (P_{val}) and the multipole parameters (P_{lm}) describing its deformation along with the corresponding expansion–compression coefficients (k, k') for each atom of the complex were obtained on the basis of the calculated structural amplitudes for the cubic cell using the MoPro program [17]. The obtained values of P_{val}, P_{lm}, k, and k' were used (but were not refined) to refine the coordinates and thermal parameters of atoms by the experimental reflections ($\sin\theta/\lambda = 0.7$ Å^{-1}) in the real symmetry of complex **Ib**.

In addition, we performed two calculations without geometry optimization for a molecule of complex **Ia** in different functionals and basis sets using the Gaussian 09 program [28]. The B3LYP/aug-cc-pVDZ [21–25] was used for complex **Ic**, and M06/ Def2TZVP was applied for complex **Id** [30, 31]. The procedure for obtaining the whole-molecule invariom was similar to that described above.

The main crystallographic characteristics and X-ray diffraction experimental parameters for complexes **I** (low-resolution study), **Ia** (high-resolution study in the multipole model), and **II** (high-resolution study in the model of independent atoms) are presented in Table 1. The R factors and residual electron densities for complexes **Ib–Id** are given in Table 2. The structures were deposited with the Cambridge Crystallographic Data Centre (CIF files CCDC 1900920 (**I**), 1900921 (**Ia**), and 1900922 (**II**); http://www.ccdc.cam.ac.uk/data_request/cif).

RESULTS AND DISCUSSION

As mentioned above, the purpose of this study is to compare the experimental (high-resolution X-ray diffraction studies) and experimental–theoretical (using the whole-molecule invariom) topological characteristics of the electron density in complex **Ia**. The molecular structure of complex **Ia** is presented in Fig. 1. The geometric characteristics of complex **Ia** are typical of compounds of this class [32–36]. Therefore, we concentrated our attention on differences in distances in the coordination sphere of the chromium atom obtained from the high-resolution X-ray diffraction analysis data (complex **Ia**) and whole-molecule invariom (**Ib**; isolated molecule geometry was optimized and **Ic**, **Id**; isolated geometry molecule was not optimized) (Table 3). An analysis of the Cr–C distances shows that the distances in the coordination sphere of the chromium atom in complexes **Ib–Id** coincide, on the whole, with similar distances in complex **Ia** within 3σ. Somewhat higher differences are observed for the C–O distances.

An analysis of the deformation electron density (DED) distribution in complexes **Ia–Id** visually indicates a substantial similarity between the experimental and experimental–theoretical DED (Fig. 2).

An analysis of the populations of the d orbitals [37] in complexes **Ib–Id** indicates a good coincidence between them regardless of the functional, basis set, and geometry optimization (Table 4). The populations of the d orbitals in complex **Ia** agree at the qualitative level with those in complexes **Ib–Id**, but there are noticeable distinctions in experimental populations of the d orbitals in compounds **Ia** and $(\eta^6\text{-}C_6H_6)Cr(CO)_3$ [32]. Note that the orbitals d_{z^2} (A representation), d_{xz}, d_{yz} (E_1 representation), d_{xy}, and $d_{x^2-y^2}$ (E_2 representation) are involved in σ-, π-, and δ-binding with the arene ligand, respectively. The highest divergence is

Table 1. Selected crystallographic characteristics and parameters of X-ray diffraction experiments for the model of independent atoms (**I**, **II**) and multipole refinement model (**Ia**)

Parameter	Value		
	I	**Ia**	**II**
Empirical formula	$C_{15}H_{15}NO_5Cr$	$C_{15}H_{15}NO_5Cr$	$C_{15}H_{15}NO_5Cr$
FW	341.28	341.28	341.28
Crystal system	Triclinic	Triclinic	Triclinic
Space group	$P\bar{1}$	$P\bar{1}$	$P\bar{1}$
a, Å	6.4602(2)	6.4624(3)	6.4624(3)
b, Å	9.9433(4)	9.9490(4)	9.9490(4)
c, Å	12.0218(4)	12.0279(5)	12.0279(5)
α, deg	72.683(2)	72.671(1)	72.671(1)
β, deg	75.565(1)	75.557(1)	75.557(1)
γ, deg	76.251(1)	76.243(1)	76.243(1)
V, Å^3	702.70(4)	703.62(5)	703.62(5)
Z	2	2	2
ρ_{calc}, g cm^{-3}	1.613	1.611	1.611
μ, mm^{-1}	0.838	0.837	0.837
F(000)	352	352	352
Crystal size, mm	0.35 × 0.35 × 0.08	0.35 × 0.35 × 0.08	0.35 × 0.35 × 0.08
Range of θ, deg	2.45–30.29	2.45–51.43	2.45–54.52
Number of collected/ Independent reflections	10101/184	197001/14034	197001/17491
R_1/wR_2 ($I > 2\sigma(I)$)	0.0300/0.0768	0.0246/0.0177	0.0365/0.0935
GOOF	1.034	0.991	1.042
Residual electron density (max/min), e Å^{-3}	0.479/–0.484	0.727/–0.747	1.611/–1.174

Table 2. Values of *R* factors and residual electron density in complexes **Ib–Id**

Parameter	**Ib**	**Ic**	**Id**
R_1/wR_2 ($I > 2\sigma(I)$)	0.0244/0.0241	0.0296/0.0322	0.0313/0.0346
GOOF	0.991	0.991	0.991
ρ_{max}/ρ_{min}, e Å^{-3}	0.36/–0.39	0.38/–0.49	0.36/–0.52

observed in the populations of the d_{yz} orbitals between complexes **Ia** and $(\eta^6\text{-}C_6H_6)Cr(CO)_3$.

An analysis of the main topological characteristics of the electron density at the critical points (3, –1) (CP(3, –1)) on the Cr–C_{CO} bonds (Table 3) shows that in complex **Id** these characteristics are insignificantly better consistent with the experimental ones (**Ia**) than in complexes **Ib** and **Ic**. In turn, when describing nondirected Cr–C_{arene} interactions, it is seen that complexes **Ic** and **Id** show the same topological characteristics of the electron density at the CP(3, –1). These characteristics somewhat better coincide with the experimental values than those in complex **Ib**. However, when comparing the topological characteristics of the electron density on the C–O bonds, complex **Ib** shows a better coincidence with the topological characteristics in complex **Ia** than complexes **Ic** and **Id**. Nevertheless, the sign of $\nabla^2\rho(\mathbf{r})$ on the C–O bonds is negative in all complexes (**Ia–Id**). It should be mentioned that the quantum chemical calculations do not always reproduce the sign of $\nabla^2\rho(\mathbf{r})$ on the C–O bonds [32, 33].

The experimental and experimental–theoretical topological characteristics of complexes **Ia–Id** are well

Table 3. Selected geometric and topological characteristics of complexes **Ia–Id***

Bond	Distance, Å	$\nu(\mathbf{r})$, a.u.	$\rho(\mathbf{r})$, a.u.	$\nabla^2\rho(\mathbf{r})$, a.u.	$h_e(\mathbf{r})$, a.u.
Cr(1)–C(1)	1.8508(4) [1.8518(12)] (1.8504(16)) {1.8482(17)}	–0.265 [–0.230] (–0.230) {–0.234}	0.144 [0.129] (0.129) {0.131}	0.464 [0.498] (0.491) {0.493}	–0.075 [–0.053] (–0.054) {–0.055}
Cr(1)–C(2)	1.8468(4) [1.8502(12)] (1.8483(15)) {1.8471(17)}	–0.248 [–0.231] (–0.230) {–0.234}	0.138 [0.129] (0.129) {0.130}	0.429 [0.503] (0.495) {0.495}	–0.070 [–0.053] (–0.053) {–0.055}
Cr(1)–C(3)	1.8387(4) [1.8401(12)] (1.8392(15)) {1.8374(17)}	–0.269 [–0.240] (–0.240) {–0.244}	0.145 [0.132] (0.133) {0.134}	0.462 [0.507] (0.504) {0.505}	–0.077 [–0.056] (–0.057) {–0.059}
Cr(1)–C(4)	2.2346(4) [2.2392(11)] (2.2351(14)) {2.2353(15)}				
Cr(1)–C(5)	2.2241(4) [2.2245(11)] (2.2218(15)) {2.2207(16)}	[–0.069] (–0.072) {–0.073}	[0.058] (0.061) {0.061}	[0.224] (0.227) {0.226}	[–0.007] (–0.008) {–0.008}
Cr(1)–C(6)	2.2219(5) [2.2199(11)] (2.2161(15)) {2.2155(16)}	–0.085 [–0.069] (–0.072) {–0.072}	0.069 [0.058] (0.060) {0.060}	0.227 [0.219] (0.223) {0.223}	–0.014 [–0.007] (–0.008) {–0.008}
Cr(1)–C(7)	2.2087(4) [2.2114(11)] (2.2075(15)) {2.2072(16)}	{–0.072}	{0.061}	{0.226}	{–0.008}
Cr(1)–C(8)	2.2175(4) [2.2204(11)] (2.2149(14)) {2.2150(15)}	–0.083 [–0.070] (–0.072) {–0.072}	0.067 [0.059] (0.060) {0.060}	0.222 [0.223] (0.227) {0.226}	–0.009 [–0.007] (–0.008) {–0.008}
Cr(1)–C(9)	2.2351(4) [2.2379(11)] (2.2347(14)) {2.2347(15)}	[–0.068] (–0.068) {–0.068}	[0.058] (0.058) {0.058}	[0.218] (0.218) {0.217}	[–0.007] (–0.007) {–0.007}
O(1)–C(1)	1.1570(6) [1.1486(14)] (1.1497(19)) {1.153(2)}	–1.622 [–1.606] (–1.610) {–1.640}	0.472 [0.471] (0.475) {0.481}	–0.263 [–0.373] (–0.582) {–0.656}	–0.844 [–0.850] (–0.878) {–0.902}
O(2)–C(2)	1.1596(6) [1.1487(14)] (1.1491(18)) {1.150(2)}	–1.609 [–1.605] (–1.612) {–1.652}	0.470 [0.471] (0.474) {0.481}	–0.307 [–0.375] (–0.523) {–0.556}	–0.843 [–0.850] (–0.871) {–0.896}
O(3)–C(3)	1.1605(5) [1.1549(13)] (1.1533(18)) {1.1560(19)}	–1.605 [–1.575] (–1.581) {–1.614}	0.470 [0.467] (0.470) {0.476}	–0.320 [–0.471] (–0.595) {–0.651}	–0.842 [–0.846] (–0.865) {–0.888}

* The geometric and topological characteristics of complex **Ia** are given without any parentheses, those of complex **Ib** are given in brackets, those of complex **Ic** are presented in parentheses, and the characteristics of complex **Id** are given in braces.

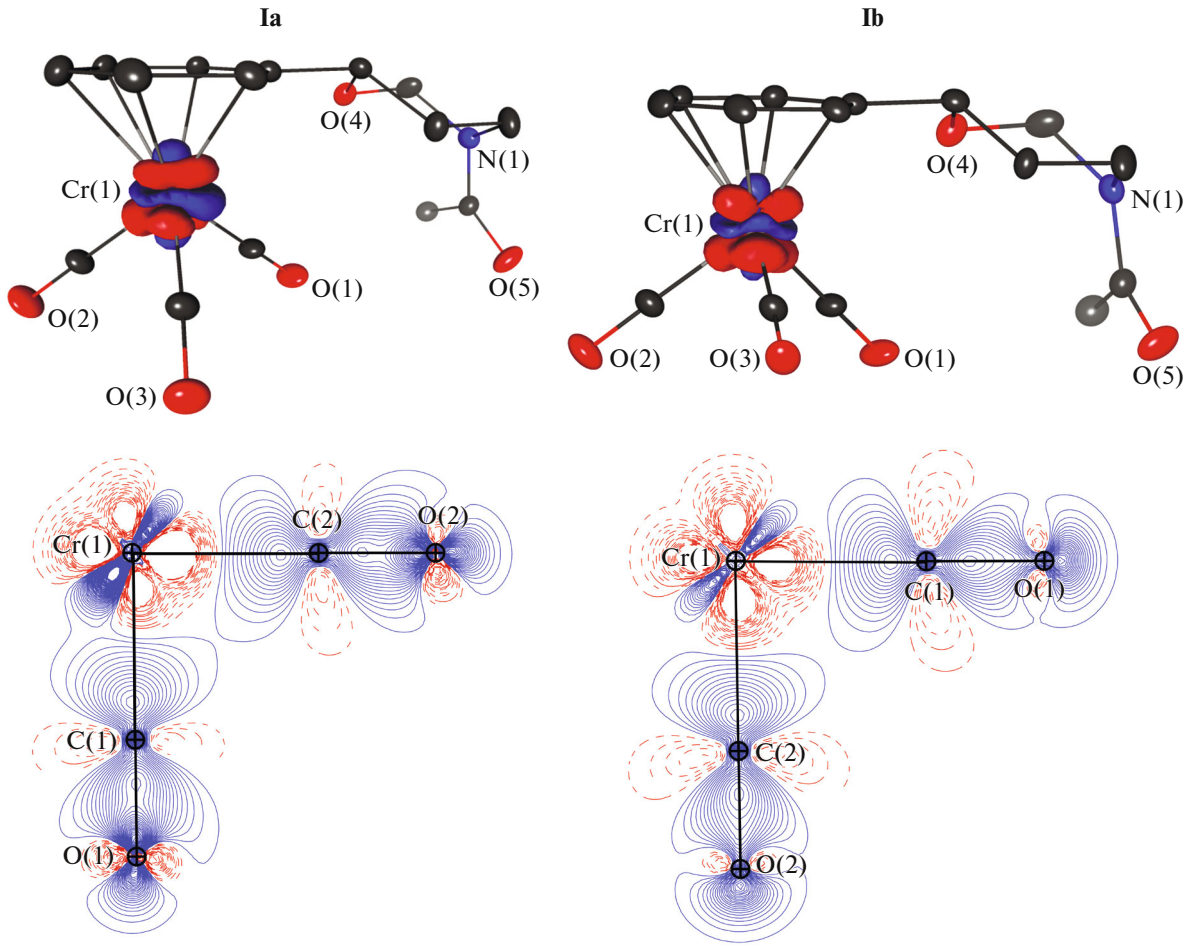

Fig. 2. Distribution of the DED in complexes **Ia** and **Ib**: the DED isosurface (0.03 a.u.) near the Cr(1) atoms and the section (±0.05 e/Å^3) in the O(1)Cr(1)O(2) plane. Solid lines show the concentration, and dashed lines show the DED depletion. Analogous isosurfaces and DED sections for complexes **Ic** and **Id** are omitted because of similarity.

consistent with similar values for $(\eta^6\text{-}C_6H_6)Cr(CO)_3$ [32] and $(\eta^6\text{-Pcp})Cr(CO)_3$ (Pcp = [2.2]paracyclophane) [38]. In addition, all values of $\rho(\mathbf{r})$ and $\nabla^2\rho(\mathbf{r})$ in complexes **Ia–Id** (except for $\nabla^2\rho(\mathbf{r})$ on the C–O bonds in **Ic** and **Id**) lie within the range of transferability indices of these values ($\rho(\mathbf{r}) = 0.1$ e Å^{-3} (0.15 a.u.), $\nabla^2\rho(\mathbf{r}) = 4$ e Å^{-5} (0.17 a.u.)) [39].

The molecular graphs of complexes **Ia–Id** are presented in Fig. 3. The visual analysis reveals two distinctions between them. The first one is presented by different numbers of bonding paths and CP(3, –1) between the Cr(1) atom and arene fragment of the molecule. The bonding paths Cr(1)–C(5) and Cr(1)–C(9) take place in complexes **Ib** and **Ic** in addition to the bonding paths (Cr(1)–C(6) and Cr(1)–C(8)) in

Table 4. Populations of the *d* orbitals in complexes **Ia–Id** and $(\eta^6\text{-}C_6H_6)Cr(CO)_3$

d Orbitals	**Ia**	**Ib**	**Ic**	**Id**	$(\eta^6\text{-}C_6H_6)Cr(CO)_3$
d_{z^2}	1.21	1.05	1.04	1.04	1.225(8)
d_{xz}	0.63	0.74	0.74	0.75	0.450(8)
d_{yz}	1.48	1.37	1.37	1.34	0.441(8)
$d_{x^2-y^2}$	1.08	0.95	0.98	0.97	0.820(8)
d_{xy}	1.28	1.19	1.18	1.18	0.822(8)

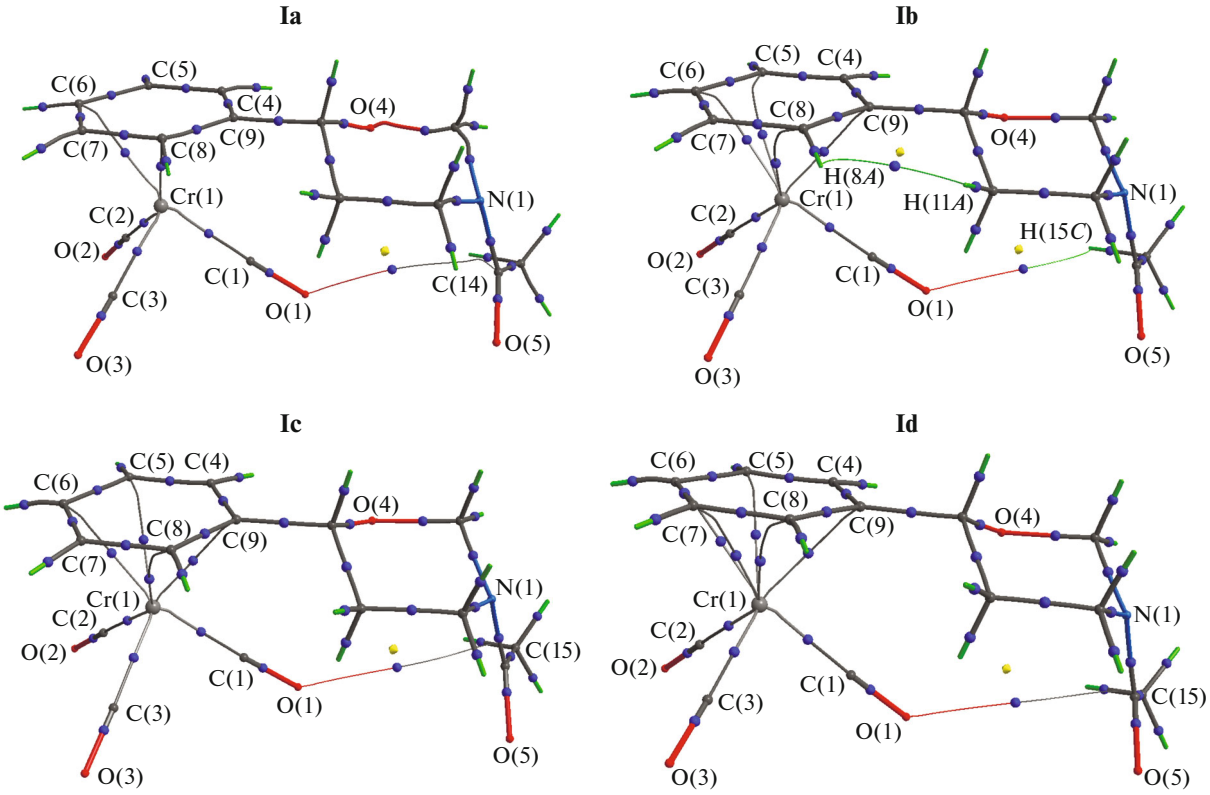

Fig. 3. Molecular graphs of complexes **Ia–Id**. Only the Cp(3, –1) and selected Cp(3, +1) are presented for clarity.

complex **Ia**. In turn, the Cr(1)–C(7) bonding path is observed in complex **Id** in addition to the paths indicated above. This situation for the 3*d*-metal complexes with carbocyclic ligands is well known [32, 33, 40–44] and is caused by a low curvature of the electron density between the metal atom and arene ligand.

The second distinction is presented by the different numbers of intramolecular interactions found in complexes **Ia–Id**. According to the molecular graphs, one intramolecular interaction O(1)···C(14) takes place in complex **Ia**, whereas two such interactions are observed in complex **Ib** (H(8*A*)···H(11*A*), O(1)···H(15*C*)). The O(1)···C(15) intramolecular interaction is observed in complexes **Ic** and **Id**.

It should be mentioned that CP(3, +1) are localized near the corresponding CP(3, –1). In other words, the situation is close to a catastrophe: the disappearance of the CP(3, –1) and the corresponding bonding paths. It is most likely that this is a reason for the absence of the bonding path H(8*A*)···H(11*A*) in complexes **Ia**, **Ic**, and **Id** and somewhat differed intramolecular interactions between the O(1) atom and C(O)Me fragment of the complexes. Evidently, either other descriptors of the presence of interactions [45–49], or other models for finding critical points [50] should be used for the reliable characterization of these interactions.

An analysis of the atomic charges (Table 5) shows that in complex **Ia** the charge on the chromium atom obtained experimentally is appreciably less positive than the charges obtained in the model of molecular invarioms (**Ib–Id**). In turn, an excellent concordance between the charges on the carbon atoms of the carbonyl groups is observed for all complexes (**Ia–Id**). The charges on these atoms in complex **Ib** coincide with the experimental values (**Ia**) within ~8%, which is somewhat exacter than in complexes **Ic** and **Id**. A less unambiguous situation is observed for the charges on the carbon atoms of the arene ligand (C(4)–C(9)). The charges on the C(4) and C(5) atoms in complexes **Ic** and **Id** reproduce similar values of charges in complex **Ia**. However, the charges for the C(6)–C(9) atoms differ substantially up to the noncoinciding sign of the charge (C(9) atom). The combined analysis of the atomic volumes and charges shows that the difference in volumes of the C(1)–C(3) carbon atoms in complexes **Ia–Id** does not exceed ~3%, and the maximum difference in charges of these atoms is ~11%. In turn, the difference in volumes of the C(6)–C(9) atoms is considerably higher. For example, the difference in volumes between the C(6) atom in complexes **Ia** and **Ib** (**Ia** and **Ic**) is ~27% (~21%), and the charges on these atoms differ by ~86% (~60%). Thus, the better the coincidence of the volumes of atoms obtained in different models (**Ia–Ic**), the better the agreement

Table 5. Charges and volumes of atoms in the coordination sphere of the Cr atom in complexes **Ia–Id***

Atom	Cr(1)	C(1)	C(2)	C(3)	C(4)	C(5)	C(6)	C(7)	C(8)	C(9)
Charge, e	0.54	0.77	0.75	0.76	−0.22	−0.32	−0.71	−0.13	−0.60	0.20
	[1.0]	[0.81]	[0.81]	[0.82]	[−0.13]	[−0.10]	[−0.10]	[−0.08]	[−0.12]	[−0.07]
	(1.0)	(0.84)	(0.84)	(0.83)	(−0.28)	(−0.24)	(−0.28)	(−0.24)	(−0.29)	(−0.02)
	{1.01}	{0.85}	{0.86}	{0.84}	{−0.29}	{−0.25}	{−0.29}	{−0.25}	{−0.30}	{−0.027}
Volume, Å^3	9.03	11.27	11.57	11.62	11.11	12.20	14.61	11.13	14.13	7.95
	[8.77]	[11.32]	[11.71]	[11.74]	[10.39]	[10.63]	[10.64]	[10.12]	[10.75]	[8.40]
	(8.85)	(11.66)	(11.95)	(12.00)	(10.81)	(11.15)	(11.53)	(10.65)	(11.63)	(8.27)
	{8.82}	{11.54}	{11.80}	{11.91}	{10.89}	{11.23}	{11.67}	{10.78}	{11.76}	{8.30}

* The charges and volumes of atoms in complex **Ia** are given without any parentheses, those for complex **Ib** are given in brackets, those for complex **Ic** are presented in parentheses, and those for complex **Id** are given in braces.

Table 6. Charges and volumes of the heteroatoms in complexes **Ia–Id***

Atom	O(1)	O(2)	O(3)	O(4)	O(5)	N(1)
Charge, e	−1.31	−1.30	−1.29	−1.20	−0.87	−1.02
	[−1.22]	[−1.20]	[−1.19]	[−0.87]	[−0.98]	[−0.89]
	(−1.16)	(−1.15)	(−1.13)	(−0.80)	(−0.90)	(−0.84)
	{−1.19}	{−1.18}	{−1.16}	{−0.83}	{−0.91}	{−0.84}
Volume, Å^3	22.09	21.14	20.85	14.26	19.79	10.61
	[21.36]	[20.80]	[20.13]	[12.96]	[18.61]	[10.83]
	(22.65)	(21.75)	(21.59)	(13.41)	(21.31)	(10.97)
	{22.03}	{21.80}	{21.61}	{13.46}	{20.52}	{11.04}

* The charges and volumes of atoms in complex **Ia** are given without any parentheses, those for complex **Ib** are given in brackets, those for complex **Ic** are presented in parentheses, and those for complex **Id** are given in braces.

between the atomic charges. Therefore, a question arises about the principal difference between the carbon atoms of the CO groups and arene substituents. Obviously, the principal difference is the character of interaction with the chromium atom. The interactions between the chromium atom and carbonyl carbon is directed (covalent, Table 3), whereas the interaction with the arene ligand is not directed (delocalized) and is characterized by a low curvature of the electron density. As mentioned previously, this results in difficulties of the localization of the CP(3, −1) in the metal–arene system. Two CP(3, −1) are localized between the chromium atom and arene ligand in complex **Ia**, whereas three, four, and five CP(3, −1) were found in complexes **Ib–Id**, respectively. Perhaps, this results in a noticeable difference in volumes of the arene C(4)–C(8) atoms, which have the same environments, in complex **Ia**, and the C(9) atom has different environment. The difference in volumes of the arene C(4)–C(8) atoms in complex **Ia** is ~24%. In complexes **Ib–Id**, the difference in volumes of similar atoms is substantially lower and does not exceed ~8%. This results in the situation where the differences in charges on these atoms are ~38% (**Ib**) and ~17% (**Ic**, **Id**). Thus, the accuracy of determination of the atomic basin plays the key role in the determination of atomic charges. In turn, all "expected" CP(3, −1) should be found for the maximum high-precision determination of the atomic basin volume. Therefore, we believe that the atomic charges in the arene ligand of complex **Id** are more realistic than those in complex **Ia**.

To confirm this hypothesis, we analyzed the values of charges and atomic volumes for all oxygen and nitrogen atoms in complexes **Ia–Id** (Table 6). The difference in charges of the heteroatoms in complexes **Ib–Id** (except for (O(4) in **Ib**) does not exceed 0.18 e. The maximum difference (0.4 e) is observed for the charges of the O(4) atoms in complexes **Ia** and **Ib**. In addition, these atoms are characterized by the maximum difference in volumes. Perhaps, this is due to the optimized geometry of complex **Ib**.

Thus, in this work, we showed for η^6-[3-acetyltetrahydro-6-phenyl-2*H*-1,3-oxazine]tricarbonylchromium(0) that the molecular invarioms describe the topological characteristics of the electron density ($\rho(\mathbf{r})$, $\nabla^2\rho(\mathbf{r})$) at the CP(3, −1) within the range of

transferability indices. In addition, it is shown that for the well determined atomic basins (almost all "expected" CP(3, −1) were found) the charges of atoms obtained from the molecular invarioms coincide with the experimental values within ~0.2 e. Note that the geometry optimization (**Ib**) gives no substantial advantages for the description of the topological parameters at the CP(3, −1), except for the values of $\nabla^2\rho(\mathbf{r})$ on the C–O bonds and insignificantly higher values of ρ_{max}/ρ_{min} (0.36/−0.39 e Å^{-3}) compared to the calculations without geometry optimization.

ACKNOWLEDGMENTS

The authors are grateful to the Center for Collective Use "Analytical Center of the Razuvaev Institute of Organometallic Chemistry of the Russian Academy of Sciences" for the use of scientific equipment.

FUNDING

This work was supported by the Russian Science Foundation, project no. 17-73-20302.

REFERENCES

1. Gatti, C. and Matta, C.F., *Modern Charge-Density Analysis*, Heidelberg: Springer, 2012.
2. Dittrich, B. and Matta, C.F., *IUCrJ*, 2014, vol. 1, p. 457.
3. Dittrich, B., Koritsnszky, T., and Luger, P., *Angew. Chem., Int. Ed. Engl.*, 2004, vol. 43, p. 2718.
4. Nelyubina, Y.V., Korlyukov, A.A., and Lyssenko, K.A., *Chem.-Eur. J.*, 2014, vol. 20, no. 23, p. 6978.
5. Nelyubina, Y.V. and Lyssenko, K.A., *Chem.-Eur. J.*, 2015, vol. 21, no. 27, p. 9733.
6. Nelyubina, Y.V., Korlyukov, A.A., Lyssenko, K.A., et al., *Inorg. Chem.*, 2017, vol. 56, no. 8, p. 4688.
7. Nelyubina, Y.V., Ananyev, I.V., Novikov, V.V., et al., *RSC Adv.*, 2016, vol. 6, no. 94, p. 91694.
8. Wandtke, C.M., Weil, M., Simpson, J., et al., *Acta Crystallogr., Sect. B: Struct. Sci. Cryst. Eng. Mater.*, 2017, vol. 73, p. 794.
9. Dittrich, B., Wandtke, C.M., Meents, A., et al., *ChemPhysChem*, 2015, vol. 16, p. 412.
10. Malischewski, M., Seppelt, K., Sutter, J., et al., *Angew. Chem.*, Int. Ed. Engl., 2017, vol. 56, no. 43, p. 13372.
11. Dittrich, B., Ruf, E., and Meller, T., *Struct. Chem.*, 2017, vol. 28, p. 1333.
12. Meisel, S.L., Dickert, J.J., and Hartoug, H.D., *J. Am. Chem. Soc.*, 1975, vol. 78, p. 4782.
13. *SAINT. Data Reduction and Correction Program, Version 8.27B*, Madison: Bruker AXS Inc., 2014.
14. Sheldrick, G.M., *SADABS-2012/1. Bruker/Siemens Area Detector Absorption Correction Program*, Madison: Bruker AXS, 2012.
15. Sheldrick, G.M., *SHELXTL V.6.14. Structure Determination Software Suite*, Madison: Bruker AXS, 2003.
16. Hansen, N.K. and Coppens, P., *Acta Crystallogr., Sect. A: Cryst. Phys., Diffr., Theor. Gen. Crystallogr.,* 1978, vol. 34, no. 6, p. 909.
17. Jelsch, C., Guillot, B., Lagoutte, A., et al., *J. Appl. Crystallogr.*, 2005, vol. 38, no. 1, p. 38.
18. Allen, F.H., Kennard, O., Watson, D.G., et al., *J. Chem. Soc., Perkin Trans.*, 1987, no. 12, p. 2.
19. Hirshfeld, F., *Acta Crystallogr., Sect. A: Cryst. Phys., Diffr., Theor. Gen. Crystallogr.*, 1976, vol. 32, no. 2, p. 239.
20. Stash, A. and Tsirelson, V., *J. Appl. Crystallogr.*, 2002, vol. 35, no. 3, p. 371.
21. Becke, A.D., *J. Chem. Phys.*, 1993, vol. 98, p. 5648.
22. Lee, C., Yang, W., and Parr, R.G., *Phys. Rev. B*, 1988, vol. 37, p. 785.
23. Stephens, P.J., Devlin, F.J., Chabalowski, C.F., et al., *J. Phys. Chem.*, 1994, vol. 98, p. 11623.
24. Balabanov, N.B. and Peterson, K.A., *J. Chem. Phys.*, 2005, vol. 123, p. 64107.
25. Balabanov, N.B. and Peterson, K.A., *J. Chem. Phys.*, 2006, vol. 125, p. 74110.
26. Grimme, S., Antony, J., Ehrlich, S., et al., *J. Chem. Phys.*, 2010, vol. 132, p. 154104.
27. Grimme, S., Ehrlich, S., and Goerigk, L., *J. Comput. Chem.*, 2011, vol. 32, p. 1456.
28. Frisch, M.J., Trucks, G.W., Schlegel, H.B., et al., *Gaussian 09. Revision D.01*, Wallingford: Gaussian Inc., 2009.
29. Jayatilaka, D. and Grimwood, D.J., *Comput. Sci. ICCS*, 2003, vol. 2660, p. 142.
30. Zhao, Y. and Truhlar, D.G., *Theor. Chem. Acc.*, 2006, vol. 120, nos. 1–3, p. 215.
31. Weigend, F. and Ahlrichs, R., *Phys. Chem. Chem. Phys.*, 2005, vol. 7, p. 3297.
32. Farrugia, L.J., Evans, C., Lentz, D., et al., *J. Am. Chem. Soc.*, 2009, vol. 131, p. 1251.
33. Fukin, G.K., Cherkasov, A.V., Zarovkina, N.Yu., et al., *Chem. Select.*, 2016, vol. 1, p. 5014.
34. Artemov, A.N., Sazonova, E.V., Krylova, N.A., et al., *Izv. Akad. Nauk. Ser. Khim.*, 2018, no. 5, p. 884.
35. Wang, Y., Angermund, K., Goddard, R., et al., *J. Am. Chem. Soc.*, 1987, vol. 109, p. 587.
36. Zarovkina, N.Yu., Sazonova, E.V., Artemov, A.N., et al., *Izv. Akad. Nauk. Ser. Khim.*, 2014, no. 4, p. 970.
37. Holladay, A., Leung, P., and Coppens, P., *Acta Crystallogr., Sect. A: Found. Crystllogr.*, 1983, vol. 39, no. 3, p. 377.
38. Kovalenko, A.A., Nelyubina, Yu.V., Korlyukov, A.A., et al., *Z. Kristallogr. Cryst. Mater.*, 2018, vol. 233, no. 5, p. 317.
39. Checińska, L., Mebs, S., Hübschle, C.B., et al., *Org. Biomol. Chem.*, 2006, vol. 4, p. 3242.
40. Scherer, W., Eickerling, G., Tafipolsky, M., et al., *Chem. Commun.*, 2006, p. 2986.
41. Smol'yakov, A.F., Dolgushin, F.M., Ginzburg, A.G., et al., *J. Mol. Struct.*, 2012, vol. 1014, p. 81.
42. Smol'yakov, A.F., Dolgushin, F.M., and Antipin, M.Yu., *Izv. Akad. Nauk. Ser. Khim.*, 2012, no. 12, p. 2185.

43. Borissova, A., Antipin, Yu., Perekalin, D., et al., *CrystEngComm*, 2008, vol. 10, p. 827.
44. Borissova, A., Antipin, Yu., and Lyssenko, K., *J. Phys. Chem.*, 2009, vol. 113, p. 10845.
45. Bader, R.W.F. and Gatti, C, *Chem. Phys. Lett.*, 1998, vol. 287, p. 233.
46. Farrugia, L.J. and Macchi, P., *J. Phys. Chem. A*, 2009, vol. 113, p. 10058.
47. Gatti, C., *Electron Density and Chemical Bonding II*, Stalke, D., Ed., Berlin: Springer, 2012, vol. 147, p. 193.
48. Farrugia, L.J. and Macchi, P., *The Chemical Bond. Fundamental Aspects of Chemical Bonding*, Frenking, G. and Shaik, S., Weinheim (Germany): Wiley, 2014, p. 127.
49. Farrugia, L.J., Evans, C., Senn, H.M., et al., *Organometallics*, 2012, vol. 31, p. 2559.
50. Anan'ev, I.V., Medvedev, M.G., Aldoshinm, S.M., et al., *Izv. Akad. Nauk. Ser. Khim.*, 2016, no. 6, p. 1473.

Translated by E. Yablonskaya